The Impact of Electrodes Arrangement on ESP Efficiency

Haidar K. Dhayef[1*], Thamir H. Khalaf[2]

Abstract

In the last few decades, electrostatic precipitators (ESP) have been improvement and many new methods have been implemented to increase in term of Particles collection efficiency in the sub micrometer size range. electrostatic precipitators rely on corona discharge processes to remove airborne dust particles. To understand particle behavior and flow dynamics inside electrostatic precipitators, a precise measurement of the electric field and charge density distribution is required. The electric field and charge density distributions in the negative wire-to-duct electrostatic precipitator were calculated using Poisson and charge conservation equations. typical efficiency of ESP as a function of geometrical and operation factors. In this paper, ESP designed and simulated using COMSOL Multiphysics® 5.5. The effects of the distance between discharge-wires on collection efficiency was studied.

Key Words: Electrostatic Precipitator, ESP, Corona Discharge, Particle Collection Efficiency, Space Charge.

DOI Number: 10.14704/nq.2022.20.2.NQ22020 **NeuroQuantology 2022; 20(2):23-31**

Introduction

There are many factors that pollute the environment and threaten life on our planet. The most important of which are air pollution resulting from toxic substances emitted from factories (such as cement factories, electric power plants, etc.). The electrostatic precipitators as the most effective way to purify toxic gases emitted from factories, such as the wire-plate electrostatic precipitator, which is characterized by its ability to pass the largest amount of gas inside it (J.H. Turner, 1999). An electrostatic precipitator is a particle control device that uses electrostatic force to remove particles out of a flowing gas stream (James H. Turner, 1988, Kenneth Parker and Norman Plaks, 2004). K. Adamiak, (1993) uses the simulation way to find the electrical properties of an electrostatic precipitator with two parallel plates and wire corona discharge electrode.

Corona discharge is now employed in a variety of industrial and technological applications, including ozone separators, powder coatings and sprays, and electrostatic precipitators, among others (M. Horenstein, 1984). The simulation of a wire-plate electrostatic precipitator with corona discharge is the focus of this paper. The principle of electrostatic precipitator using corona discharge phenomenon can be described as:

A high-intensity electric field is applied between a high-curvature corona electrode (wire) and a low-end curvature collecting electrode (plate), allowing gas molecules in close proximity to the corona electrode's surface to be ionized. The interaction space is separated into two distinct regions: the high-field ionization region, which surrounds the active electrode where free charges are created, and the low-field drift region, which takes up the rest of the space.

Corresponding author: Haidar K. Dhayef
Address: [1*]College of Science, University of Sumer, Iraq; [2]Department of Physics, College of Science, University of Baghdad, Iraq.
[1*]E-mail: a86athr@yahoo.com

Relevant conflicts of interest/financial disclosures: The authors declare that the research was conducted in the absence of any commercial or financial relationships that could be construed as a potential conflict of interest.
Received: 28 November 2021 **Accepted:** 30 December 2021

The electrons travel towards the positive electrode represented by the collector plate and are neutralized when a negative corona surrounds the wire. It is also pushed away from the corona negative electrode by the electric field. As a result, the particles are charged and collect on the collecting plates.
When airborne particles enter and pass through the gas ion pathways, the ions cling to them, giving them a negative charge. Because most particles are huge compared to gas particles, so the charge seems negligible at the beginning of the charge of particles. Many gas ions, on the other hand, can fit on a particle, and they do. Smaller particles with a diameter of (less than 1 micrometer) can contain tens of ions (Gao, 2019 Bouazza, 2018), while larger particles with a diameter (greater than 10 micrometers) can absorb tens of thousands of ions. In the end, after the particle acquires a certain number of ions, the particles emit their negative electric field, which works to repel other gas ions, and consequently no additional ions are obtained, and this is the meaning of saturation. Now the negatively charged particles are subjected to the force of electrostatic attraction to pull it strongly. Larger particles have more charges, so the saturation charge is higher. Thus it is pulled more forcefully to the grounded board. In other words, it travels faster than smaller particles.

Description of the Model and Equations

Static electricity, laminar flow, and particle tracking are the three physics modules that make up an ESP's core concepts (M. Johansen, 2018). Each module is solved sequentially:

1. Laminar Flow

To solve the components of the velocity and pressure in the model domain, the Navier-Stokes equation is used:

$$\rho(u.\nabla)u = \nabla.[-pI + \mu(\nabla u + (\nabla u)^T)] + F_{EHD} \quad (1)$$

Where μ is the dynamic viscosity, ρ is the fluid density, p if the pressure, and F_{EHD} is the electro-hydrodynamic force define as:

$$F_{EHD} = \rho_q E \quad (2)$$

2. Electrostatics

The static electric field is solved by the electrostatic module, by combining the electric potential, the constitutive relationship equation and Gauss's law, and this allows us to produce the Poisson equation (Sui, 2016).

$$\nabla.E = \rho/\varepsilon_0 \quad (3)$$

$$E = -\nabla V \quad (4)$$

$$\varepsilon_0 \nabla^2 V = -\rho \quad (5)$$

Where ρ is the space charge number density, **E** is the electric field, $\boldsymbol{V}$ is electric potential, and ε_0 is the vacuum permittivity.
The electric potential at the wire of diameter (0.5 mm) is at the highest voltage, without going into corona breakdown at the greatest voltage the corona breakdown voltage was previously measured (J. Miller,1998). The material library provides all the constants for air.

3. Particle Tracing

The results of the previous two modules provide the charge of the particles, the electric field strength and the aerodynamic strength of the particle tracking module.
Following Newton's second law, the particle locations are determined by solving second-order equations of motion for the particle position vector components:

$$\frac{dr}{dt} = v \quad (6)$$

$$\frac{d}{dt}(m_p v) = F_t \quad (7)$$

Where r denotes the particle's position, v is the particle velocity, m_p is the particle mass and F_t is the total force acting on the particle. In this example the forces acting on the particles are the drag force and the electric force. Rarefaction effects need to be included in the drag force because the particle radius become very small. Here, the drag force F_D is described with the Cunningham-Millikan-Davis model.
The electrostatic force to which each particle is subjected is expressed as:

$$\boldsymbol{F} = q\boldsymbol{E} \quad (8)$$

Where q denotes the particle's and $\boldsymbol{E}$ denotes the electric field vector.
In general, the particle charge depends on the charge density of the corona discharge model. Negative density represents the number of electrons and negative ions that can stick to the surface of the particle to be removed. Estimates the particle charge (M. Johansen, 2018).

Results and Discussions

All numerical simulations were conducted with duct type discharge electrode connected to a dc electric potential of 20 kV. The main gas average velocity, pressure level and temperature were set to 1 [m\s], 1 [atm] and 293.15 [K] respectively. The effect of the electrodes geometry is studied on particle collection efficiency of ESP. The geometrical parameter values used in the simulated ESP design are shown in table 1. A full-scale ESP was assumed in the model simulation (Fig. 1) illustrates it. Figure (2) depicts the finite-element mesh that surrounds the corona wire and covers the area of interest. The size of the element ranges from 0.0002 [m] as the minimum and 0.0045 [m] as the maximum. The mesh has a high concentration near the corona wire, where high gradient is predicted, although the elements elsewhere can be bigger.

Table 1. Ranges of design parameters for electrostatic precipitator

name	expression	value	description
H	0.1[m]	0.1 m	Height
rin	0.5[mm]	5E-4 m	Electrode radius
w	0.7[m]	0.7 m	Width
sp	13,15,18,21,24 [cm]	0.13,0.15,0.18,0.21,0.24 m	Electrode separation

According to the separation distance between the electrodes of ESP, it was predicted to know the effect of this parameter on the performance of ESP.

previous studies have shown (Karwat B, 2016) that the most important geometric parameter determining the electric field intensity produced by the corona electrode is the distance between electrodes.

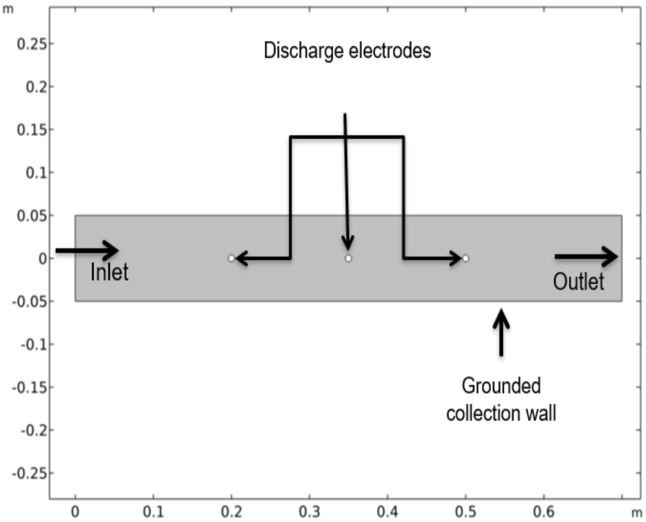

Figure 1. Simulation domain of the electrostatic precipitator (the inner electrodes are not to scale)

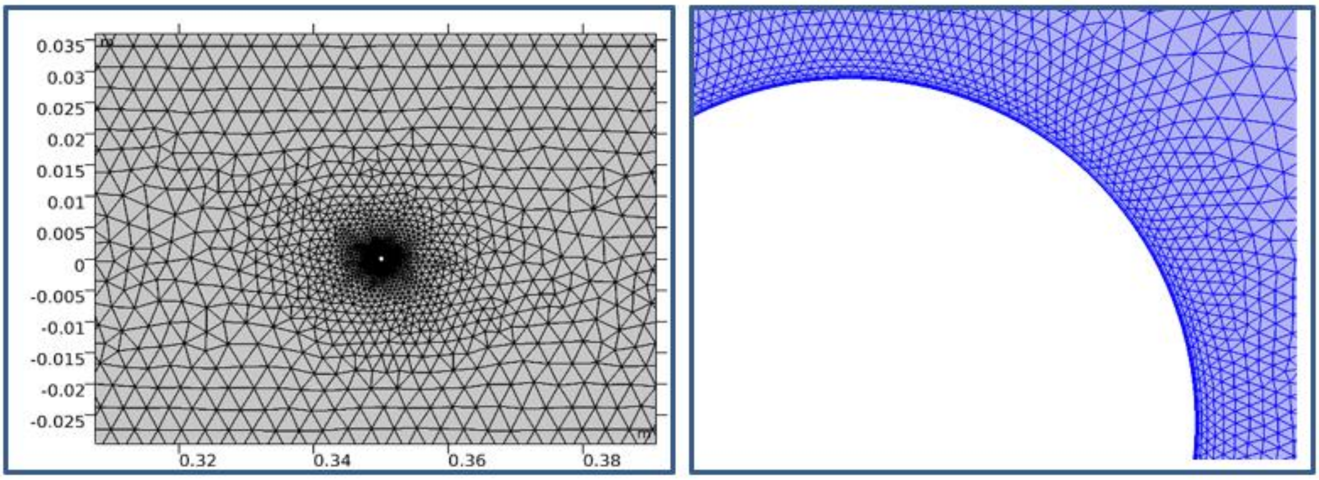

a) b)

Figure 2. The finite-element mesh for computer simulation, (a) total of mesh around discharge electrode and (b) magnification of the mesh area around the discharge electrode.

1. Electric Potential Distribution

We notice from Figure (3), which shows the computational distribution of electric voltage, that The electric field intensity is very strong near the corona wire and gradually decreases towards the grounded electrode, which is compared to the semi-empirical solution provided by (Ahmed Kasdi, 2015). At the ionization region, the electric potential is very important, as it peaks at the negative electrodes and decreases away from them, so it is zero at the surface of the grounded plate.

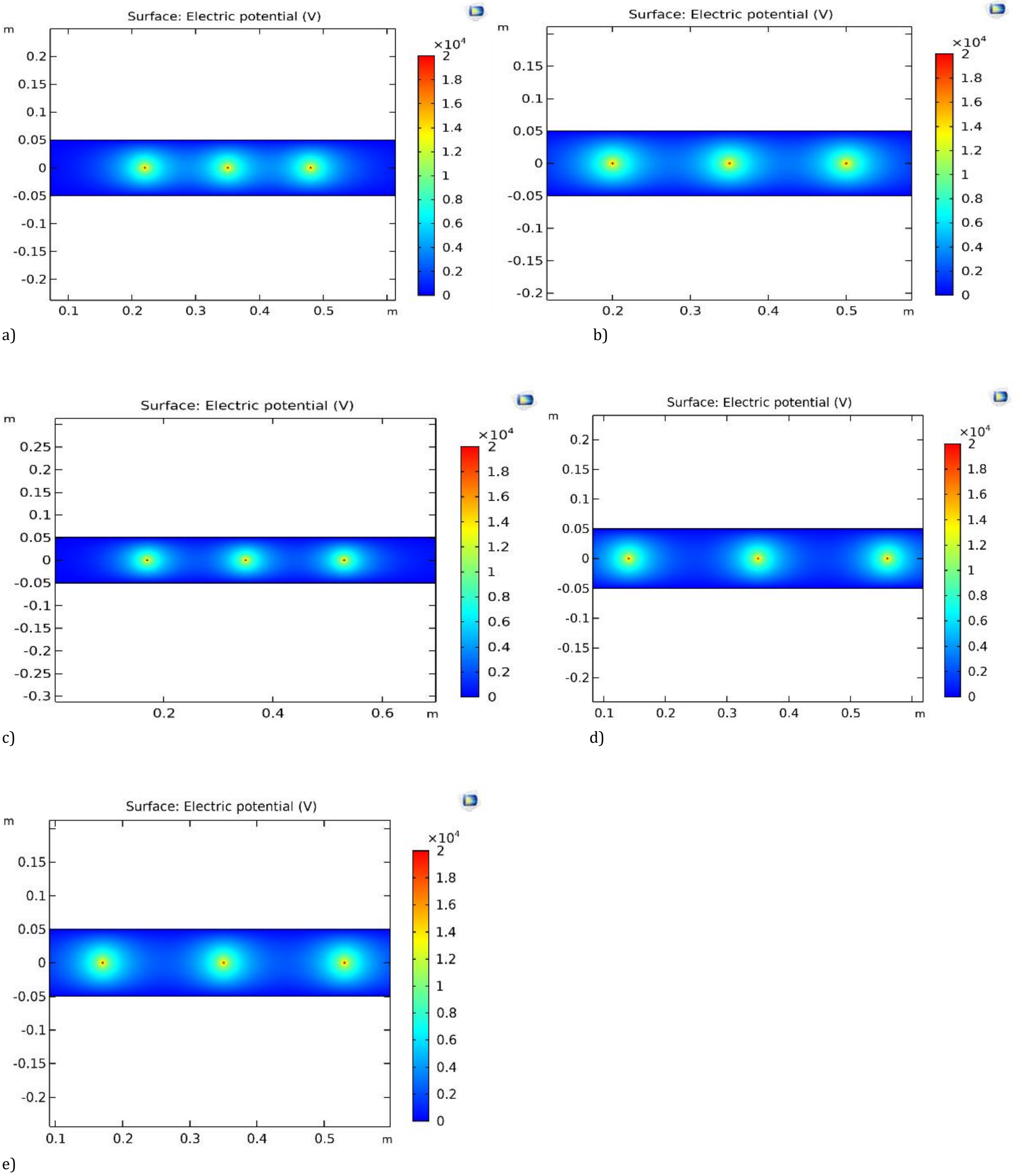

Figure 3. 2D electric potential distribution; (a) at 13[cm], (b) at 15 [cm], (c) at 18 [cm], (d) at 21 [cm], (e) at 24 [cm].

2. Space-charge Density Distribution

The effect of space charges on the electric field distribution Distributions of space charge density computed along the beam the direction is illustrated in Figure 6. And according to the distances in the figures (a, b, c, d & e) where we notice that the smaller the distance between the electrodes, the greater the possibility of charging particles, it remains constant at the surface of the wire because it is a result of Peek's assumption. According to previous studies, It is clear that the presence of space charge has an obvious effect on

NeuroQuantology | February 2022 | Volume 20 | Issue 2 | Page 23-31 | doi: 10.14704/nq.2022.20.2.NQ22020

the electric field (Ahmed Kasdi, 2015). The space charge density is more intense near the inner electrodes, as expected, where a corona discharge is luminous. It is in the regions near the inner electrodes that particles accumulate charge at a faster rate due to the combined effect of large space charge densities and intense electric fields.

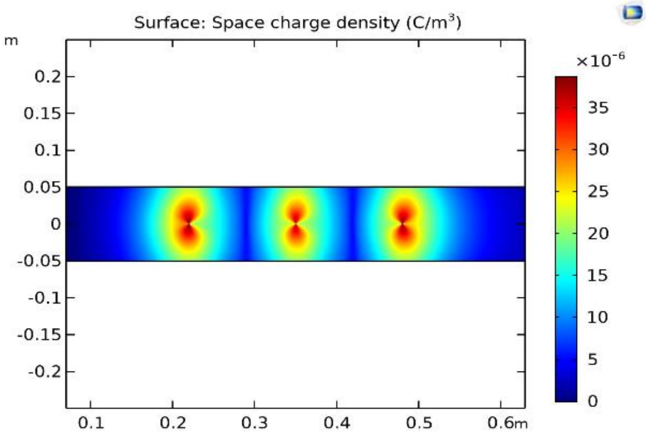

a)

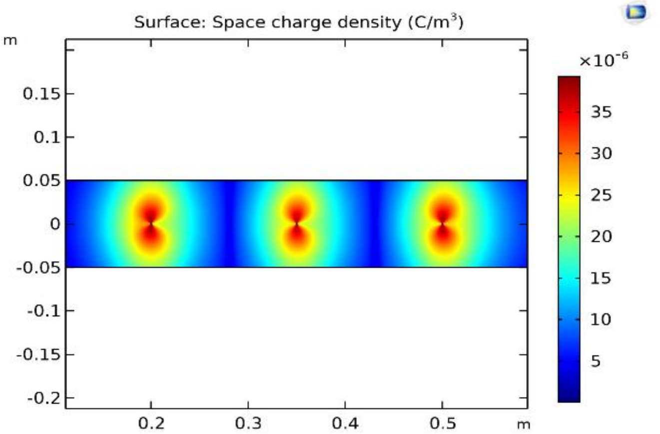

b)

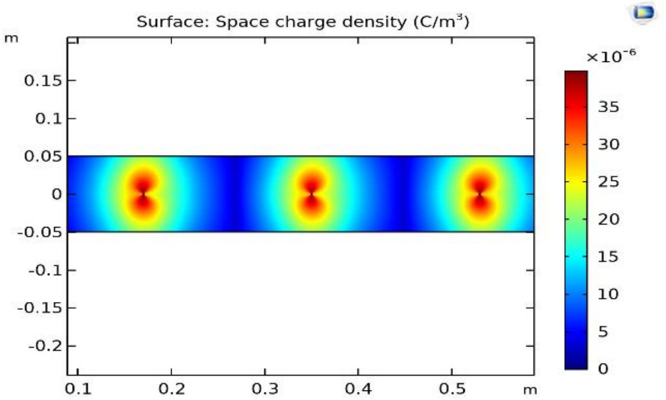

c)

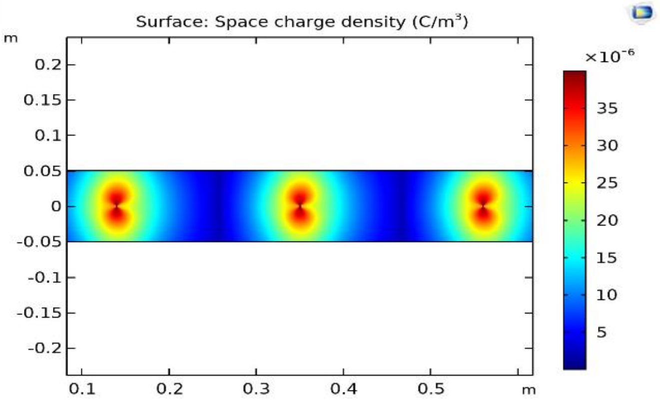

d)

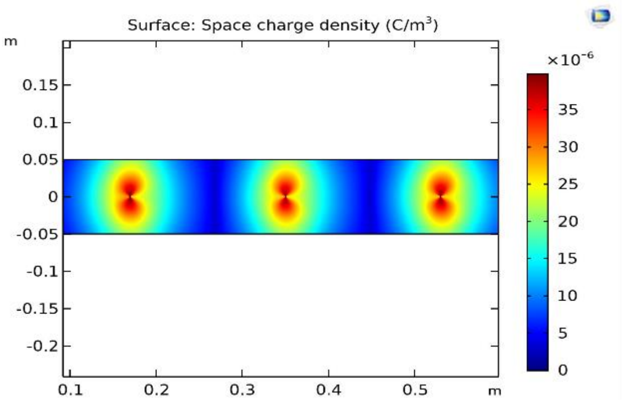

e)

Figure 4. 2D space-charge density distribution; (a) at 13[cm], (b) at 15 [cm], (c) at 18 [cm], (d) at 21 [cm], (e) at 24 [cm].

3. *Fluid Velocity*

The combined effect of the electrodes geometry and the gas flow is illustrated in figure (5). For a given electrodes curvature, the divergence of the electrical field lines depends on the distance between the negative electrodes. It is found that distance between the negative electrodes has influence on velocity of migration of particles,

*e*ISSN 1303-5150

which is an important factor in determining the efficiency of ESPs. So that, fluid velocity obtained with the corona model coupled with the Laminar Flow interface. the corona and the fluid model are fully coupled. However, model results show that the fluid velocity is practically not influence by the electro hydrodynamic force, and the drift velocity is always much larger than the fluid velocity in the regions of interest.

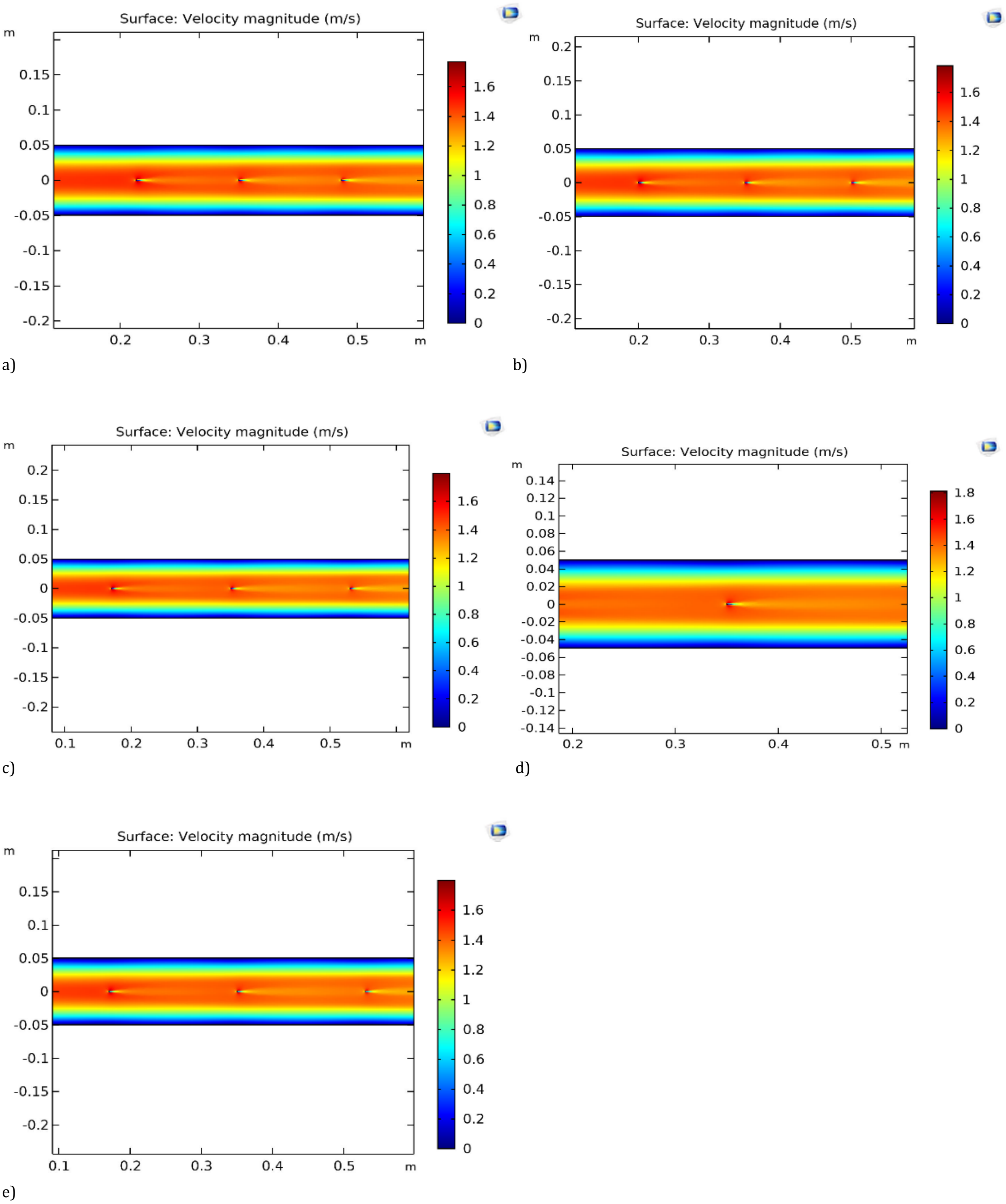

Figure 5. 2D velocity migration; (a) at 13[cm], (b) at 15 [cm], (c) at 18 [cm], (d) at 21 [cm], (e) at 24 [cm]

4. Contour Pressure

The contours in Fig. (6) illustrate an assessment of the effect of the electrodes separations on pressure. As expected, the electrostatic force acting on the particles to be collected is proportional to the pressure. The pressure contour lines were drawn in COMSOL Multiphysics software according to what is shown in the sub-figures of Figure (7).

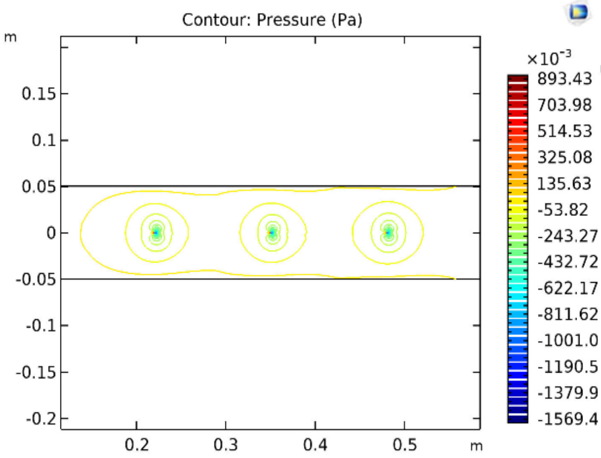

a)

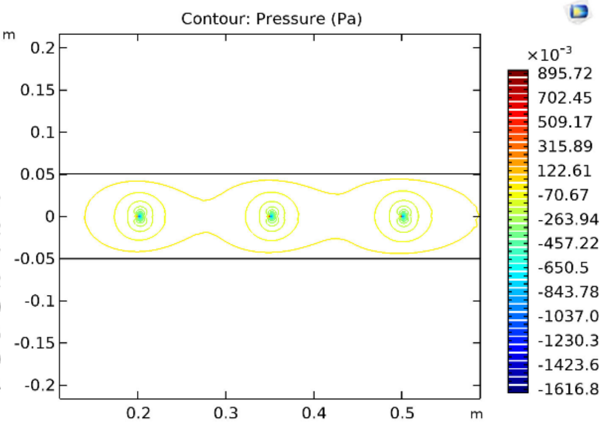

b)

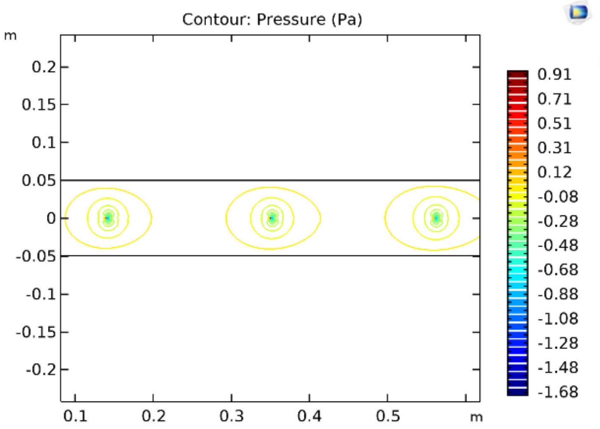

c)

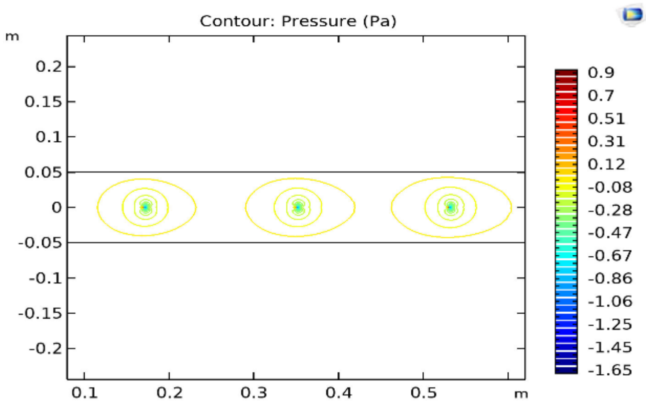

d)

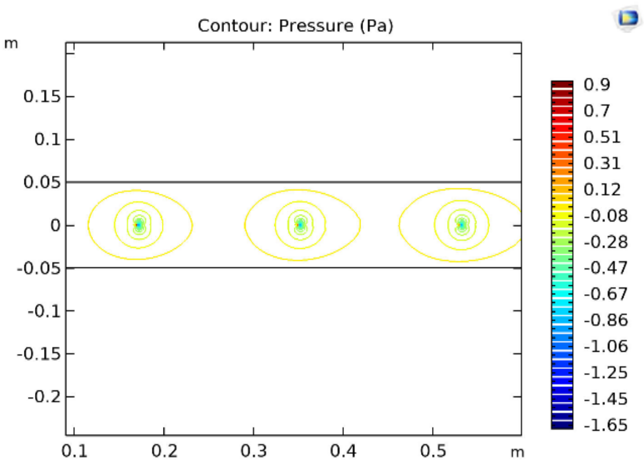

e)

Figure 6. Contour 2D pressure distribution; (a) at 13[cm], (b) at 15 [cm], (c) at 18 [cm], (d) at 21 [cm], (e) at 24 [cm]

29

5. *Collection Efficiency*

Figure (7) present the particle collection efficiency and the average particle charge at the last time step as a function of the particle radius. The collection efficiency is larger at the extremes of the particle dimensions. Larger particles are collected more efficiently because they attain greater electric charge, while smaller particles are collected more efficiently because are subjected to less drag force. Between this two extremes, the drag force influences the most the particle trajectories resulting in almost straight lines parallel to the collection plates that result in low collection efficiency. At the small particle branch partial charging becomes important. A model that correctly describes partial charging should capture the random nature in which a particle can have a charge of 1 or 0. In the present model, particles can be charged with a number between 0 and 1, which might result in inaccurate collection efficiency results for small particles.

Has proven, in comparison with the experimental results (J. Miller, 1998), that by increasing the separation distance, the particle collection efficiency decreases by stabilizing the voltage at 20 KV. This is due to the decrease in the value of the electric field, which in turn affects the concentration of particles. Predicted particle collection efficiencies for wire type discharge electrodes as a function of particle diameter. Based on the particle surface charge and cross-sectional cumulative efficiencies, Due to the high electric field and ion density in the surrounding area, field charging processes are only effective in the vicinity of DEs (Sui, 2016). Also, the corona power loss in-creases as the wire-to-wire spacing increases while keeping the voltage constant. The present agreement with the experimental results is in agreement.

By discussing the results we obtained, we find that the best values of the internal factors in the design of the electrostatic precipitator by the computer simulation method to obtain a high-efficiency precipitator at SP = 13 (cm).

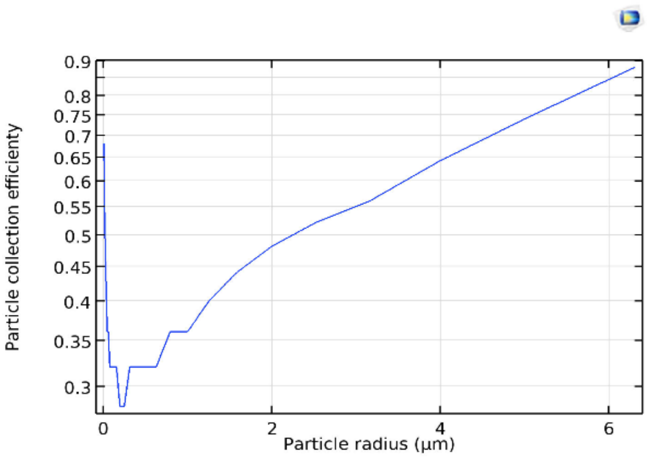

a)

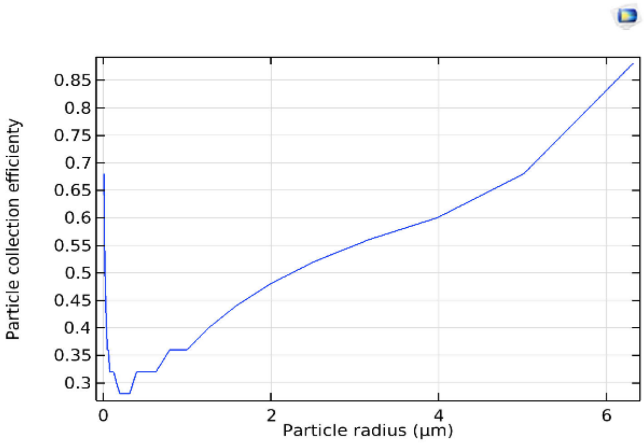

b)

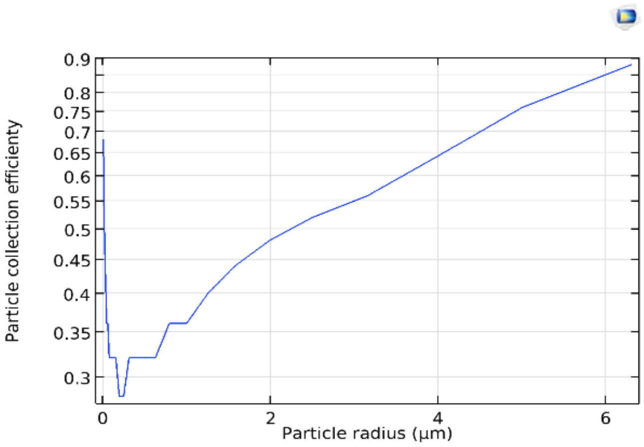

c)

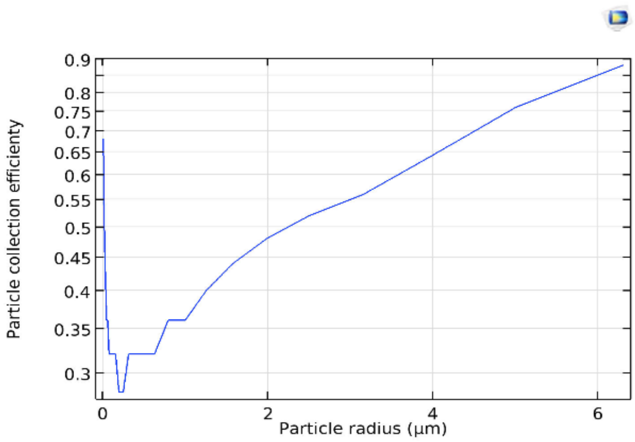

d)

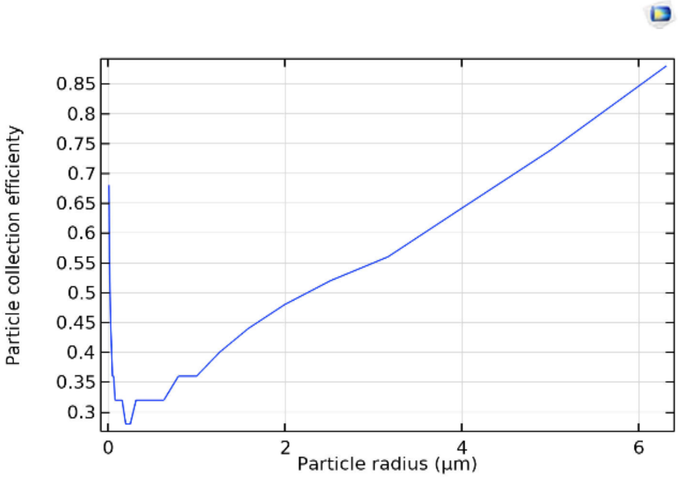

e)

Figure 7. Particle collection efficiency for wire type of ESP as a function of particle diameter versus particle radius; (a) at 13[cm], (b) at 15 [cm], (c) at 18 [cm], (d) at 21 [cm], (e) at 24 [cm]

References

Turner JH, Lawless PA et al. (1999). Electrostatic Precipitators, EPA.

James HT, Phil AL, Toshiaki Y, David WC, Gary PG, John DM, William MV. Sizing and Costing of Electrostatic Precipitators. *JAPCA* 1988; 38(4): 458-471.

Parker K, Plaks N. Electrostatic precipitator (ESP) training manual. *United States Environmental Protection Agency, Washington* 2004.

Adamiak K. Simulation of corona in wire-duct electrostatic precipitator by means of the boundary element method. *IEEE Transactions on Industry Applications* 1993; 30(2): 381-386.

Horenstein MN. Computation of corona space charge, electric field, and VI characteristic using equipotential charge shells. *IEEE transactions on industry applications* 1984; (6): 1607-1612.

Bouazza MR, Yanallah K, Pontiga F, Chen JH. A simplified formulation of wire-plate corona discharge in air: Application to the ion wind simulation. *Journal of Electrostatics* 2018; 92: 54-65.

Gao W, Wang Y, Zhang H, Guo B, Zheng C, Guo J, Yu A. Numerical simulation of particle migration in electrostatic precipitator with different electrode configurations. *Powder Technology* 2020; 361: 238-247.

Johansen MR, Phillips III JR, Wang JJ, Mulligan J, Mackey PJ, Calle CI, Clements JS. Electrical characteristics of the Mars electrostatic precipitator. *In Joint Electrostatics Conference* (No. KSC-E-DAA-TN56585) 2018.

Sui Z, Zhang Y, Peng Y, Norris P, Cao Y, Pan WP. Fine particulate matter emission and size distribution characteristics in an ultra-low emission power plant. *Fuel* 2016; 185: 863-871.

Miller J, Hoferer B, Schwab AJ. The impact of corona electrode configuration on electrostatic precipitator performance. *Journal of Electrostatics* 1998; 44(1-2): 67-75.

Karwat B, Nocuń M, Machnik R, Niedźwiedzki J. Modelling and study the effect of selected design features for the operating parameters of industrial electrostatic precipitators. *Eksploatacja i Niezawodnosc – Maintenance and Reliability* 2016; 18(3): 325–332.

Kasdi A, Zebboudj Y, Yala H. Simulation of Corona Discharge in DC Electrostatic Precipitator. *Journal of Electrical Systems* 2015; 11(4): 384-396.

Al-Sawaff ZH, Rashid ZM, Yahya YZ, Kandemirli F. Electromagnetic field smart splint for bone fixing and rehabitation using niti shape memory alloy. *NeuroQuantology* 2020; 18(3): 37-44.